nature communications

Article

https://doi.org/10.1038/s41467-026-78604-8

Spatially resolving isomeric trisaccharides on surfaces with Orbitrap-SIMS

Received: 29 April 2025

Accepted: 28 September 2026

Published online: 17 October 2026

Check for updates

Margaret Moloney[1,2], Richard Paterson[1], Bin Yan[1], Anya Eyres[1,3], Clare L. Newell[1,4], Jean-Luc Vorng[1], Alexander Pirkl[5], John F. Watts[2], Ian S. Gilmore[1] ✉ & Gustavo F. Trindade[1] ✉

Many biologically important molecules are structural isomers that share the same molecular mass yet differ in shape, bonding and function. This creates an ambiguity for mass spectrometry imaging (MSI), where chemically distinct species can be indistinguishable on the mass-to-charge (*m/z)* scale and therefore cannot be reliably mapped in heterogeneous materials. Here we demonstrate that Orbitrap secondary ion mass spectrometry (OrbiSIMS) can provide an orthogonal contrast that enables both identification and spatial separation of isomeric molecules directly on surfaces. By exploiting structure-dependent secondary-ion dissociation and gas-phase collisional effects during ion transmission, we discriminate isomeric trisaccharides raffinose, maltotriose and melezitose and spatially resolve raffinose and maltotriose in mixtures. We benchmark these measurements against ion mobility spectrometry and observe consistent trends between OrbiSIMS transmission behaviour and ion mobility separation. These results establish OrbiSIMS as an approach for isomer-resolved MSI at surfaces and interfaces, opening opportunities to map isomeric biomolecules in complex systems where spatial distribution is central to function.

Structural isomers are molecules that share the same molecular formula but differ in atomic connectivity or three-dimensional arrangement. They are a fundamental source of chemical and functional diversity in biological and technological systems. Subtle differences in bond topology or spatial organisation can give rise to markedly different physicochemical properties, intermolecular interactions and biological activities. In living systems, structural isomerism is central to processes such as molecular recognition and regulation, for example, dictating the functional roles of carbohydrates through differences in glycosidic linkage and branching or modulating the activity of lipids and metabolites with identical elemental composition[1–3]. At surfaces and interfaces, structural isomers can also influence packing motifs, crystallinity and reactivity, thereby affecting macroscopic material behaviour. Identifying and separating isomeric molecules by their higher order structure or shape, combined with their spatial localisation, can bring new biological insight, for example, understanding the function of glycans in cell walls[4] or unambiguous determination of lipid distribution within a tissue[2]. However, because structural isomers are compositionally indistinguishable while functionally distinct, directly detecting and discriminating them, particularly in heterogeneous environments, remains challenging.

Mass spectrometry imaging (MSI) has been a transformative suite of methods over the past 50 years, with current technology being able to detect and spatially map various kinds of molecules in parallel and without the use of labels. Secondary ion mass spectrometry (SIMS) is an MSI method based on the detection of ionised species resulting from the impact of a primary ion beam on a sample surface, with the ability to map in three dimensions[5]. Over the last decade, SIMS has had significant impact for biological imaging, with constant developments towards improved ion beams and analysers for biomolecules[6,7], higher

[1]National Physical Laboratory, NiCE-MSI, London, UK. [2]School of Engineering, University of Surrey, Guildford, UK. [3]Chemistry Research Laboratory, Department of Chemistry, University of Oxford, Oxford, UK. [4]The Francis Crick Institute, London, UK. [5]IONTOF GmbH, Münster, Germany.
✉e-mail: ian.gilmore@npl.co.uk; gustavo.trindade@npl.co.uk

spatial resolution, better accuracy in molecular identification, and preserving the native state with cryogenic analysis[8–10]. Orbitrap™ SIMS (OrbiSIMS, also known as Hybrid SIMS) is a recent technique that is growing in popularity in a wide range of applications in life sciences and materials science[11]. An OrbiSIMS instrument features a dual analyser configuration with a time-of-flight (ToF) analyser and an Orbitrap analyser (Fig. 1a). As a consequence, this instrument has the ability to combine the mass spectrometry performance usually found in state-of-the-art proteomics and metabolomics with fast 3D imaging at the microscale and from nanolayers of less than 1 nm of thickness, which enables molecules to be studied directly from surfaces and tissues, unlocking new capability in important applications such as proteomics[12,13], lipidomics[8,14,15], metabolomics[9,16–19] and drug delivery[18].

However, OrbiSIMS MSI is only able to detect mass-to-charge ratios (m/z), which carries only basic information of a molecule's structure. When analysing small metabolites, the ions observed are usually singly charged and the desired structural information is usually of the primary and secondary order as opposed to native protein analysis, where the ions generated are typically multiply charged and the structural information desired is often tertiary and quaternary. Therefore, other parameters such as charge distribution can also be used to infer structure (Table 1). The charge state distribution (CSD) observed correlates with the solvent-accessible surface area; typically, an increase in CSD is associated with protein unfolding[20–23]. Structural information inferred from CSD in MSI can be obtained via desorption electrospray ionisation (DESI), nanoDESI, and liquid extraction surface analysis (LESA). When no accurate spatial information is needed and samples can be prepared in solution, molecular structure can also be inferred by coupling MS with liquid chromatography for physical separation[24]. By adding additional reaction steps for fragmenting precursor molecules (tandem MS also known as MS/MS[25,26]) to infer structural information from fragmentation patterns of molecules in collision-induced, surface-induced or UV induced dissociation, or hydrogen-deuterium exchange (HDX)[27–29]. Ion mobility spectrometry (IMS) is another established method to study molecular structure, where ions of the same m/z but different shapes are separated depending on how they transit a gas-filled collision cell[30]. Differences in electrophoretic mobility of the ion in a buffer gas can be used to infer structural information; the collisional cross section measured is indicative of how compact the ion is. IMS is suitable to be coupled with the imaging capability of MSI as previously shown with matrix-assisted laser desorption ionisation (MALDI), DESI and LESA sources, allowing parallel imaging and structural information. MALDI and on-tissue chemical derivatisation have also been used to separate isomers using MSI. In current SIMS instruments, structural information can be inferred only via collision-induced dissociation (CID), leaving molecules that are intractable by this technique lacking in any secondary structural information. Table 1 contains a summary of MS-coupled techniques for inferring molecule structure.

Secondary ion emission is an energetic process resulting in fragmentation. Patterns in relative ion intensities can be specific to a particular structural isomer. However, relative intensities may vary for many reasons and so using them as a fingerprint introduces ambiguities for identification in complex samples. Recently, fragmentation patterns in SIMS have been combined with the high accuracy of the Orbitrap analyser to infer structure of proteins[12,13], biomarkers[31] and nucleotides[10]. However, there are no established methods using a SIMS platform for the direct detection, separation and 3D mapping of structural isomers on solid surfaces and interfaces.

In OrbiSIMS, for secondary ions to be efficiently transferred to the Orbitrap analyser, their potential energy is matched to the Orbitrap acceptance window by biasing the sample with a target potential (V_T) and their kinetic energy distribution from the SIMS collision process is reduced through elastic collisions with a helium gas at a pressure p_{He} (Fig. 1a). We previously conducted a systematic assessment of V_T and p_{He} on the transmitted secondary ion intensities of inorganic and organic molecules and revealed interesting patterns, indicating the possibility for additional information from secondary ion molecules[32]. Here, we explore OrbiSIMS V_T spectra and use them analytically to detect and spatially resolve the signal of mixtures of structural isomeric trisaccharides.

Results

Varying target potential selects dissociated ions

We acquired OrbiSIMS mass spectra of a reference silver sample with a scanned V_T potential (Fig. 1b) to produce V_T spectra of various clusters (Fig. 1c). Experimental details are in "Methods" and Supplementary Note 1. The standard target potential for OrbiSIMS analysis of conducting materials is $V_{T1} = 57.5$ V, which is suitable to detect all stable $[Ag_n]^+$ clusters from a reference silver sample[32]. However, if V_T values are increased up to 400 V, a more complex distribution pattern is revealed in the silver cluster intensities, with changing maxima in transmission which vary with cluster size (Fig. 1b, c and Supplementary Figs. 1.1 and 1.2). The V_T values for the multiple maxima are inversely proportional to m/z (Fig. 1d) in agreement with our model (Supplementary Note 1), which suggests that $[Ag_n]^+$ clusters are metastable and randomly dissociate at a constant rate into smaller clusters at some point before they are decelerated to enter the collision cell. Daughter molecules that result from dissociation in an electric field-free region are collectively selected by a 90-degree deflection unit in the ion optics (Fig. 1e), that acts as an energy band pass filter. Ions are therefore transmitted to the Orbitrap for a given, optimal V_T value. For singly charged molecules ($z = 1$), Eq. (1) predicts the position of all maxima, V_{T2}, for daughter ions with mass m_2 where the maximum for the parent ion with mass $m_1 = m_2 + \Delta$ is given by V_{T1}:

$$V_{T2}^{\max} = \left(V_{T1} + V_E\right) \frac{m_2}{(m_2 + \Delta)} - V_E \tag{1}$$

Where V_E is the extraction potential. For silver clusters, Δ can only be multiples of the masses of the two Ag isotopes (^{107}Ag and ^{109}Ag) and V_{T1} is the optimised potential of 57.5 V. This is sufficient to estimate all possible dissociations, and the experimental data has good agreement with the model (Fig. 1d and Supplementary Figs. 1.1 and 1.2). Selection of dissociated fragments has previously been proposed for polymer materials using electrostatic[33] and ToF[34] analysers. In addition to the well-defined peaks, V_T spectra also show an exponential background, which is a result of molecular dissociation within electric field gradients, as previously described using unimolecular dissociation models for mass spectrometry in general, including SIMS[35–39]. These models generally predict an exponential decay of the parent ions with time, with a certain rate constant depending on the dissociation[35–39]. Therefore, each V_T spectrum can be fitted to a sum of exponentially modified Gaussian curves, where the exponential tail of the asymmetric peaks create the baseline signal observed for all V_T spectra presented here. We describe the function in more detail in Supplementary Note 1. For the purposes of this work, only decays in field-free regions are considered for prediction of parent ions, therefore the model has been simplified to identify the V_T values where maxima occur due to decays.

OrbiSIMS instruments are hybrid instruments and contain a ToF analyser. Using the silver reference sample and based on previously published work[37], we conducted a similar experiment using the ToF analyser and changing the target potential (Supplementary Note 2). The ToF analyser contains a reflectron for energy focusing, which as a result, acts as a low-energy pass filter. Therefore, by scanning the target voltage we were able to obtain the integral of the daughter ions produced by metastable decay reactions after emission. By differentiating the signal, we convert the low-energy filtered ToF data into an equivalent to the V_T spectra acquired using the 90-degree deflection unit and Orbitrap analyser (Supplementary Fig. 2.1a, b). Spectral

https://doi.org/10.1038/s41467-026-78604-8

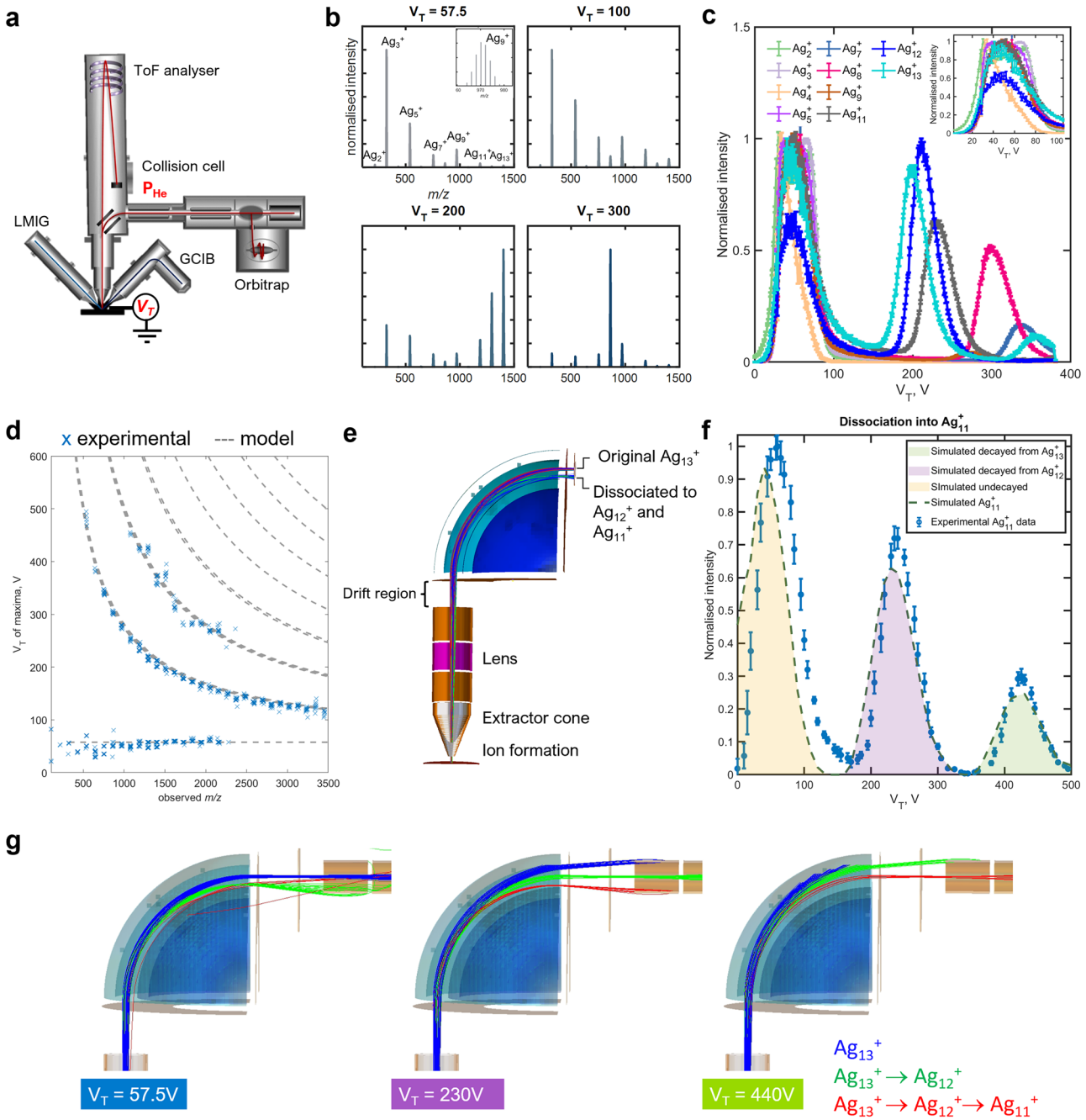


Fig. 1 | Varying target potential in OrbiSIMS selects dissociated ions. **a** Schematic of instrument showing key parameters V_T and p_{He}. (adapted from ref. 11 with permission from Springer Nature BV, Copyright 2017). **b** Mass spectra of reference silver sample at 4 different values of V_T. **c** V_T spectra (normalised to maximum intensity for each ion) of reference silver showing signal for clusters sized 1 to 11. **d** V_T values for maximum transmission in function of m/z for clusters sized up to 33. Dashed lines represent estimated values based on model of dissociation in a field-free region. **e** Ion optics simulation model with example dissociation of Ag_{13}^+ ions before they enter the 90 degrees deflector. Details of the simulation framework are in the Supplementary Information. **f** Overlay of a measured (blue), calculated (dashed green) and simulated V_T spectra for $[Ag_{11}]^+$. **g** Ion optics simulation model with example dissociation of $[Ag_{13}]^+$ ions for V_T values of 57.5, 230 and 440 V. Error bars in (**c** and **f**) represent the standard deviation across 8 to 9 sequential repeats at a given V_T before moving to the next V_T value. Images in (**e** and **g**) were 3D rendered using SIMION 8.1 and labels added using Microsoft PowerPoint. Source data are provided as a Source Data file.

resolution is coupled with the reflectron and therefore degrades (Supplementary Fig. 2.1c, d). Nevertheless, the results show the same maxima in V_T scans as the Orbitrap data and their positions are described in **Equation 1**, supporting our metastable decay model. A full comparison of the model against ToF and Orbitrap data is presented in Supplementary Note 2.

To aid the interpretation of the results on secondary ion dissociation and transmission into the Orbitrap, we established an ion optics simulation model (Fig. 1e–g, details in Supplementary Note 3). As an example, the number of simulated $[Ag_{11}]^+$ ions transmitted to the Orbitrap as a function of V_T shows good agreement with the experimental data for the same secondary ions (Fig. 1f). There is also good agreement between the simulated V_T and P map for transmission of $[Ag_{11}]^+$ with our previous metrology study[32]. The small differences are likely due to second-order effects such as kinetic energy of formation, decays inside electric field gradients (which may also lead to

Table 1 | Summary of MS-coupled techniques for inferring molecule structure

Technique coupled to MS	Lateral resolution	Method(s) of structure inference
LC	N/A	Differences in retention time induced by differential interactions with stationary and mobile phases.
CID	N/A	Dissociation of ion induced by collisions with inert gas. Fragmentation pattern informs structure. Protein CID often results in loss of a single subunit. Labile modifications to proteins are often lost.
SID	N/A	Dissociation of ion induced by collision with a surface, typically self-assembled monolayers of $CF_3(CF_2)_{10}CH_2CH_2S$ on gold[49].
UV-PD	N/A	UV photodissociation of ion. Energy absorption by ion is independent of charge state. Often used for protein-lipid complexes.
HDX	N/A	Exchange of labile hydrocarbons with deuterium in solution. Gives information on how buried/exposed amino acid residues are on a protein.
IM-MS	N/A	Differences in electrophoretic mobility in a buffer gas. Gives information on how compact the ion is.
DESI	35–50 µm[50]	On-tissue derivatisation, often coupled with IMS-MS and/or CID.
nanoDESI	10 µm[51]	On-tissue derivatisation, often coupled with IMS-MS and/or CID.
MALDI	600 nm–10 µm[52]	On-tissue derivatisation, often coupled with IMS-MS and/or CID.
LESA	400 µm–1 mm	On-tissue derivatisation, often coupled with IMS-MS and/or CID[53,54],
AutoPiMS	20 µm	Automated nanoDESI coupled with auto-CID[55].
ToF-SIMS	200 nm–1.5 µm	.Coupled with CID[56,57]
OrbiSIMS	1.5 µm	Quasi-MS/MS can be inferred from primary ion fragmentation in MS1 spectrum. Coupled with CID.

background signal in V_T spectra) and sub-optimal transmission and restrictions on the simulations[34–40]. This shall be investigated in future work.

The fact that we can separate dissociated fragments in V_T spectra, together with our previous observations on the dependency transmission of secondary ions on V_T and the collision cell pressure[32], reveal that there is potential for the study of further molecular properties using OrbiSIMS (and to some extent ToF-SIMS) that expands beyond the *m/z* scale to separate molecules based on their structure.

Structural isomers on surfaces

To investigate the potential for OrbiSIMS to separate structural isomers using V_T spectra, we studied three trisaccharide structural isomers, raffinose, maltotriose and melezitose, which have been used before to validate other approaches using IMS[41]. These have the same molecular formula $[C_{18}H_{32}O_{16}]^-$ and are detected as the $[M\text{-}H]^-$ ion but have different structures (Fig. 2a). Thin films of each sugar were spin-coated on top of a silicon wafer, to avoid electric charge build up during the analysis, and to allow for the preparation of mixtures (further details in "Methods"). The intensity of $[M\text{-}H]^-$ is not useful to distinguish between these structural isomers. V_T spectra of the $[M\text{-}H]^-$ ion at standard He cell pressure (0.04 mbar) for organic materials for each sample show that optimal transmission occurs at approximately −30 V; however, both raffinose and melezitose show multiple maxima in their V_T spectra with an oscillating pattern with clear peaks at −207, −262, −320, −375 and −435 V, which have a mean difference of 59 V. Those features are absent for maltotriose, which enables separation (Fig. 2b).

Using Eq. (1), we predicted the unit masses of potential parent ions for the $[M\text{-}H]^-$ detected at the multiple maxima of the V_T spectra. These were then used to identify peaks in the experimental mass spectra and are listed in Table 2 with their putative assignments.

The potential parent ions in Table 2 have masses higher than the molecular ion of the sugars. This indicates that they are weakly bonded to impurities in the sample or generated via recombination during the sputtering process. The identified potential parent ions are all detected as secondary ions and their V_T spectra has a maximum at −30 V (Supplementary Fig. 4.1). This indicates that they are directly formed in the secondary ion emission process.

In addition to the V_T spectra data, we also investigated the effect of the collision cell He pressure, p_{He}, with V_T set at the two values where maxima occur, −30 and −207 V and benchmarked our OrbiSIMS results with ion mobility mass spectrometry (IMS) of solutions of each compound (Fig. 2c). The intensity of the quasi-molecular ion $[M\text{-}H]^-$ has different optimal p_{He} for transmission for each of the isomers (Fig. 2d, e). This is because the collision cross-section depends on the shape of the molecule. We further expanded our ion optics simulation framework to assess transmission of secondary ions after elastic collisions with a He atom with a given collision cross section (Supplementary Note 3). The p_{He} scans do not fully resolve the trisaccharides, but the pressure for optimal transmission did match the trend in the IMS data (Fig. 2f). The IMS peak drift times of the structural isomers are inversely proportional to their respective optimal p_{He} for OrbiSIMS transmission; the lower the pressure for optimal transmission in OrbiSIMS, the longer the drift time in IMS. This is generally as expected since a lower p_{He} is used for molecules with a larger collision cross-section and these are consequently slower travelling through the IMS drift region. Previously reported cross section values are 216.3 Å^2 (maltotriose), 197.0 Å^2 (raffinose), and 203.5 Å^2 (melezitose) (PubChem database). The geometry of the collision cell is an RF ion guide, with more details in a previous publication[11]. Furthermore, the separation of ions does not rely on timing, but on transmission. The ions need to be decelerated, and the effectiveness of this deceleration depends on the collisional cross-section of the molecule and the pressure in the collision cell. The OrbiSIMS instrument also has a bent flatapole filled with N_2 gas that can vary with the He pressure[11]. Therefore, to confirm that this behaviour is ruled by He rather than N_2, we have repeated experiments allowing only He to vary (Supplementary Fig. 4.2). In all three methods (V_T spectra, varying p_{He} and IMS) a more distinct separation is found for maltotriose with raffinose and melezitose being more similar. This is in agreement with the similarities in their V_T spectra, molecular structure and collisional cross sections[41]. All three trisaccharides yield the same peaks in their OrbiSIMS spectra; however, they have different spectral patterns, which results in different relative amounts of the peaks for those secondary ion fragments formed in the SIMS process (Supplementary Fig. 4.3 and Supplementary Table 4.1). Assignments were done according to symbol nomenclature for Glycans[42,43]. Fragmentation patterns agree with published fragmentation data for hexose oligosscharides[44], and only differences in intensities allow distinction between the three trisaccharides. This agrees with previous reports on that specificity of

https://doi.org/10.1038/s41467-026-78604-8

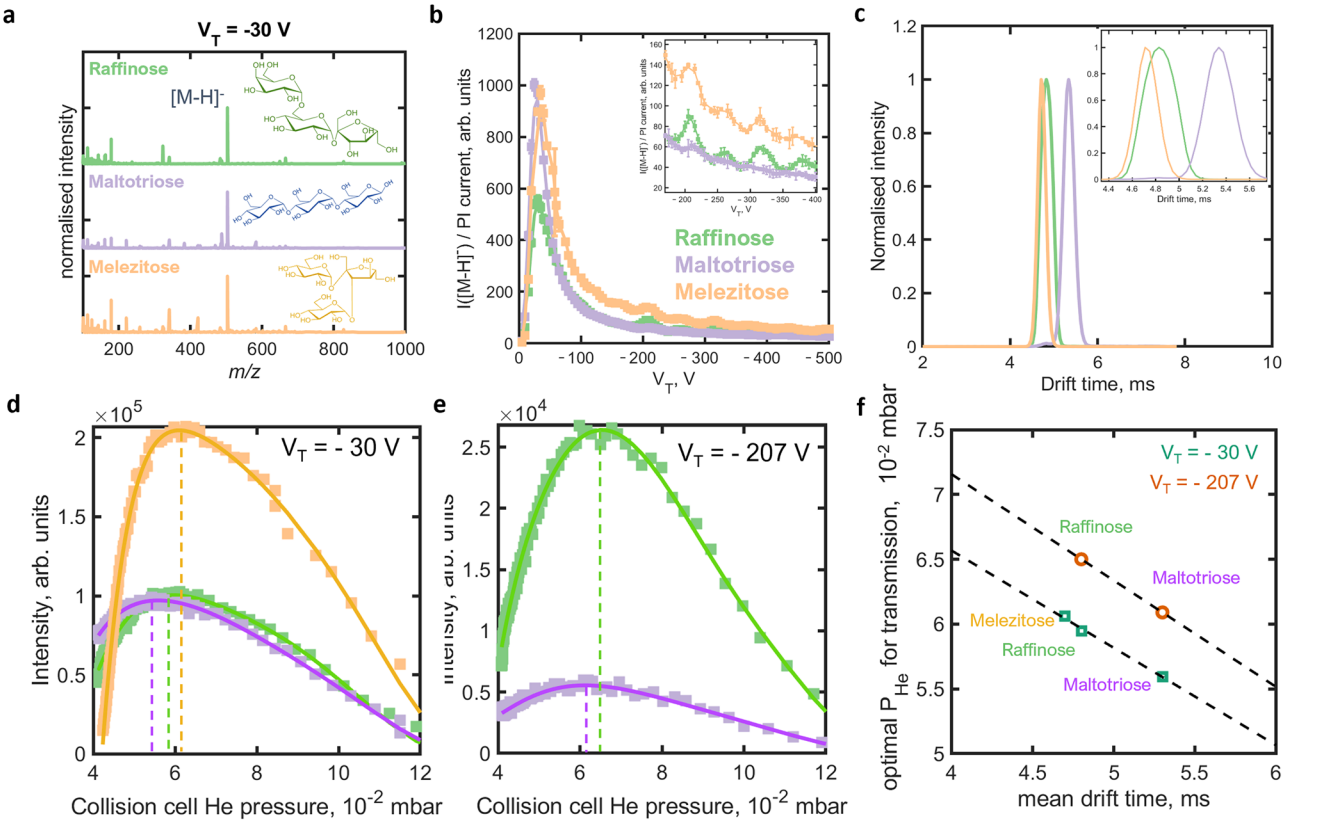


Fig. 2 | Unambiguous direct detection of structural isomeric trisaccharides. mass spectra of raffinose, maltotriose and melezitose with inset showing deprotonated quasi-molecular ion $[M\text{-}H]^-$ for each compound. **b** V_T spectra for all three compounds with inset showing a zoomed in view of intensities between V_T of −180 and −400 V. **c** IMS results for each compound. p_{He} scans at V_T values of **d** −30 V and **e** −207 V. The coloured dashed vertical lines represent the p_{He} for maximum intensity in each curve. **f** Comparison between mean drift time in the IMS results and optimal p_{He} for transmission of the molecular ion for each compound. A p_{He} scan was not acquired for melezitose at V_T = −30 V. Error bars in (**b**) represent the standard deviation across 3 to 4 sequential repeats at a given V_T before moving to the next V_T value. Source data are provided as a Source Data file.

Table 2 | Predicted unit masses of potential "parent ions" for the $[M\text{-}H]^-$ detected at the multiple maxima of V_T spectra of raffinose and melezitose and identified peaks in the experimental mass spectra

V_T of maximum (V)	Calculated parent unit mass	*m/z* in spectrum	Molecular formula	Putative assignment	Deviation (ppm)
−30	–	503.1617	$[C_{18}H_{31}O_{16}]^-$	$[M\text{-}H]^-$	−0.2
−207	547	547.1515	$[C_{19}H_{31}O_{18}]^-$	$[M\text{-}H + CO_2]^-$	−0.1
−262	561	561.1610	$[C_{20}H_{33}O_{18}]^-$	$[M\text{-}H + C_2H_2O_2]^-$	−0.4
−320	575	575.1828	$[C_{21}H_{35}O_{18}]^-$	$[M\text{-}H + C_3H_4O_2]^-$	−0.1
−375	589	589.1985	$[C_{22}H_{37}O_{18}]^-$	$[M\text{-}H + C_4H_6O_2]^-$	−0.1
−435	603	603.2141	$[C_{23}H_{39}O_{18}]^-$	$[M\text{-}H + C_5H_8O_2]^-$	−0.2

fragmentation patterns in SIMS enables identification of glycosaminoglycans[45] and allows for validation of separation of individual trisaccharides, however separation of isomers within a mixture or complex biological system remains challenging. As shown in Supplementary Note 2, the ToF analyser can be used to produce V_T spectra for each sample $[M\text{-}H]^-$ ion. Ideally, an argon gas cluster primary ion beam should be used with the ToF analyser for a direct comparison against the Orbitrap analyser; however, due to beam-pulsing limitations of the specific instrument used in this study, only a Bi_n^+ primary ion beam can be used for ToF analysis, which results in low ion yield and noisy signal even at optimal transmission conditions.

Mixtures of structural isomers

To assess whether the signal from isomers could be resolved and be relatively quantified in a mixture, we prepared thin film samples of 1:1 and 2:1 mixtures of raffinose and maltotriose and performed V_T and p_{He} scans (at V_T = −26 and −220 V) using the same conditions as before (Fig. 3a, b). At −220 V, the optimal p_{He} for transmission of the $[M\text{-}H]^-$ ion varies approximately linearly with the % of raffinose in the mixture. Whereas at −26 V, the p_{He} initially increases linearly, but after 60% drops (Fig. 3c).

In the V_T spectra of mixtures, the oscillating features of the $[M\text{-}H]^-$ ion that are characteristic of raffinose are present, as well as the distinguishing maxima of $[C_{14}H_{23}O_{12}]^-$ and $[C_6H_{11}O_6]^-$ at −345 V (Fig. 3d, e). Those features can be used to check whether the signal from the mixtures shows a linear proportion to the amount of each compound. Figure 3g shows the V_T spectrum for $[C_6H_{11}O_6]^-$ in the range of −250 to −450 V for pure raffinose and maltotriose, revealing two distinct peaks for raffinose and one for maltotriose. These peak shapes are then used to fit to the V_T spectra for the two mixtures (Fig. 3g). For each V_T spectrum, an exponential background was removed prior to fitting.

Peak fitting to each mixture's V_T spectrum was conducted by fixing the V_T peak centres and peak widths and allowing the peak areas to vary. Qualitatively, the mixtures present features from both isomers, but the areas of the fitted peaks do not have a linear correspondence to the proportions in the mixture. A possible reasons for this non-linearity is the effect of ion suppression, which are well characterised in binary mixtures[46,47]. Details of the fitting are in "Methods" and a table with all fitted parameters are in Supplementary Note 5.

Spatially resolving mixtures of structural isomers on surfaces

To establish whether OrbiSIMS can spatially resolve structural isomers, we first optimised imaging conditions for raffinose and maltotriose drop deposited next to each other on the same and different substrates without mixing. Results show that imaging with different V_T values yield different $[M\text{-}H]^-$ signal intensities, with raffinose having a relatively stronger signal at −205 and −315 V in agreement to their V_T spectra (Supplementary Figs. 6.1–6.4). We also used the relatively strong $[C_{14}H_{23}O_{12}]^-$ signal for maltotriose (Fig. 3e and Supplementary Fig. 6.2) as an internal control for the presence of maltotriose, which helps to validate the V_T method.

When the two isomers were deposited on the same substrate and allowed to touch, the fact that they have a common solvent (DI water), meant that there was an area where raffinose and maltotriose mixed, with potential migration of one sugar into the area of the other (Fig. 4a). We confirmed that, for similar molar concentrations, the structural isomers raffinose and maltotriose on the same substrate can be spatially distinguished via OrbiSIMS imaging with different V_T values (Fig. 4b–d, f). The intensity of the $[M\text{-}H]^-$ ion in the raffinose area is clearly enhanced relative to the maltotriose area as V_T is changed. (Fig. 4b–d). The intensity profile across the area where the raffinose and maltotriose have mixed (Fig. 4f) shows a factor of four enhancement of the raffinose $[M\text{-}H]^-$ intensity relative to the maltotriose intensity for V_T −205 V, in agreement with the imaging data acquired for samples deposited on the same substrate but not touching and therefore not mixing (Supplementary Note 6).

Fragmentation patterns also helped to establish the presence of the two sugars and a ground truth for the imaging dataset (Supplementary Fig. 6.5). At −25 V, using the $[C_{14}H_{23}O_{12}]^-$, the maltotriose area is shown in the bottom right of the sample and using the $[C_{12}H_{21}O_{11}]^-$, the raffinose area is the top and the left section of the sample. The fragmentation pattern is therefore confirming the area that contains the raffinose. This is not a conclusion that only raffinose is present in these parts, visual inspection when the samples were being made showed that the raffinose flowed into some of the area that had originally been only maltotriose (which had been deposited the day before, was dry and pinned to the substrate) and it is assumed that maltotriose also flowed back into the raffinose sample given they had a common solvent. The ToF-SIMS image for the $[M\text{-}H]^-$ and $[C_{14}H_{23}O_{12}]^-$ ions also indicates maltotriose is in the bottom right of the sample (Fig. 4e and Supplementary Fig. 6.5). The much lower $[M\text{-}H]^-$ signal intensity for the ToF data in relation to the Orbitrap data is due to a lower molecular ion yield from the 30 keV Bi_3^+ primary ion beam compared with the 20 keV Ar_{3500}^+ primary beam used for Orbitrap data. Differences in fragmentation patterns might not exist for other structural isomers. making the target potential parameter, V_T, rather than the fragmentation pattern, an additional variable to exploit.

Discussion

In this work, we demonstrate that OrbiSIMS can resolve and spatially map structural isomers by exploiting ion transmission behaviour rather than relying on m/z alone. Specifically, we show that the combination of target potential (V_T) and collision cell pressure (p_{He}) introduces a new analytical dimension that enables discrimination of isomeric trisaccharides that are otherwise indistinguishable. Our results establish that ions detected at a given m/z do not arise exclusively from intact molecular ions, but also from a distribution of higher-mass precursor species that undergo metastable decay during ion transmission. These decay pathways and their relative contributions differ between structural isomers, possibly due to differences in steric availability for adduct bonding, thus producing characteristic V_T transmission profiles that can be used for identification and spatial mapping without surface modification. Ions are likely to fragment randomly with a constant decay rate; those that decay in a field-free region retain the velocity of their precursor, resulting in distinct transmission maxima as a function of V_T. These maxima therefore carry information about the parent-daughter fragment relationship and, indirectly, molecular structure. Our modelling and simulation framework supports this interpretation, showing that transmission maxima correspond to metastable decay processes occurring during ion transfer. Importantly, this mechanism introduces a post-source dissociation-like dimension within a SIMS workflow, without requiring explicit MS/MS acquisition.

This transmission-based separation shares conceptual similarities with established approaches such as IMS and post-source dissociation, where structural information is inferred from gas-phase behaviour and fragmentation pathways. OrbiSIMS combines direct surface sensitivity, high spatial resolution imaging and structure-sensitive transmission behaviour within a single experiment. Our benchmarking with IMS shows that optimal p_{He} correlates with ion mobility drift times, supporting that collisional cross section, and therefore molecular shape, contributes to transmission behaviour. This suggests that OrbiSIMS transmission encodes complementary structural information to IMS, but in a manner compatible with direct surface and volume imaging.

A key implication of this work is that structural isomers can be distinguished using the quasi-molecular ion $[M\text{-}H]^-$ alone, even when fragmentation patterns are similar or ambiguous. This is particularly important for molecules such as lipids, glycans and metabolites, where isomerism is present, but fragmentation signatures may overlap. This is also highly relevant when analysing small polar metabolites, where structural isomers are abundant, whose fragmentation patterns often fall below the m/z cutoff of Orbitrap mass analysers. The ability to distinguish these in a spatial manner would enable in depth analysis of a range of disease states governed by differences in isomeric small metabolites.

We further demonstrate that this approach can be extended to mixtures and spatially resolved systems. V_T-dependent imaging enables localisation of isomers on surfaces, even in partially mixed regions, by selectively enhancing signals from specific species. Although quantification remains challenging due to matrix effects and ion suppression, the results show that transmission behaviour can be used qualitatively, and potentially semi-quantitatively, to distinguish components in heterogeneous systems. This capability is particularly relevant for applications where spatial organisation is critical, such as biological tissues, biofilms and functional interfaces.

Some aspects of the mechanism require further investigation. First, the full distribution of precursor species contributing to a given detected ion remains unclear, including the origin and stability of adduct species. Second, while our model captures dissociation in field-free regions, dissociation occurring within electric field gradients contributes to the observed exponential background and is not yet fully described analytically. Third, the role of matrix effects in mixtures and their dependence on V_T introduces non-linearity that currently limits quantitative interpretation. Finally, it remains to be established how general this behaviour is across different molecular classes and whether it consistently enables isomer separation beyond the model trisaccharides studied here. The approach can be complementary to CID-based methods, in particular for small isomeric molecules which may have their fragmentation pattern fall under the m/z 50 lower limit of Orbitrap analysers.

https://doi.org/10.1038/s41467-026-78604-8

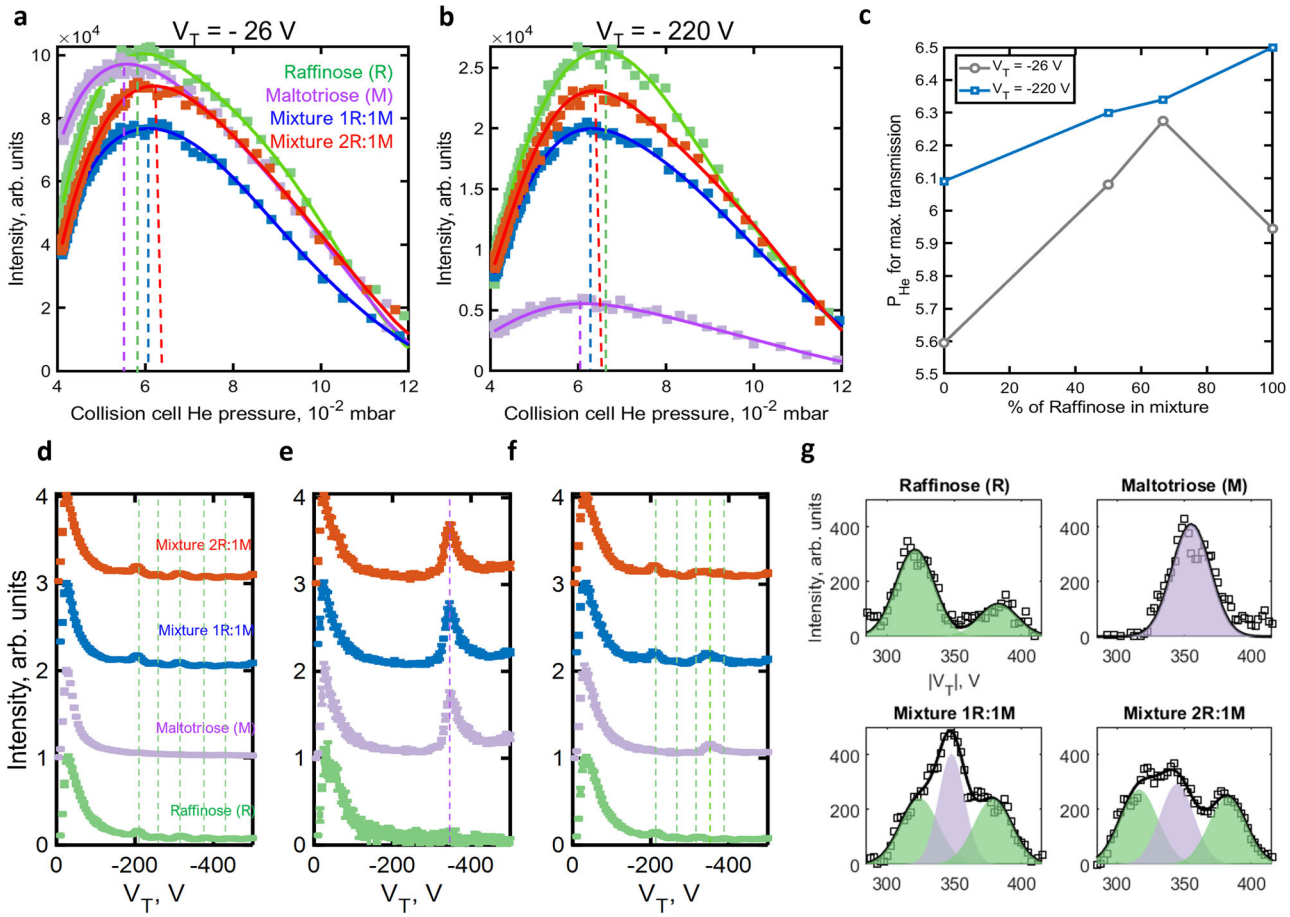


Fig. 3 | Identifying structural isomeric trisaccharides in mixtures. p_{He} scans for pure raffinose, pure maltotriose and 1:1 and 2:1 mixtures at **a** V_T = −30 V and **b** V_T = −207 V. The coloured dashed vertical lines in (**a**, **b**) represent the P_{He} for maximum intensity in each curve. **c** p_{He} for maximum transmission in function of % of raffinose in the mixture. V_T spectra at p_{He} = 0.04 mbar for pure samples and mixtures showing intensities of **d** $[C_{18}H_{31}O_{16}]^-$, **e** $[C_{14}H_{23}O_{12}]^-$ and **f** $[C_6H_{11}O_6]^-$. The dashed vertical lines in (**d**–**f**) represent the V_T for intensity local maxima. **g** Relative quantification of V_T spectrum signal in mixtures based on $[C_6H_{11}O_6]^-$ signal for pure samples. Source data are provided as a Source Data file.

We showed that a ToF analyser with a reflectron can also be used to produce V_T spectra and data matched the dissociation model, validated using silver clusters. Mass resolution is degraded with increasing V_T spectrum and this can be challenging for complex samples. To produce energy-specific data using the ToF analyser, one must differentiate the signal resulting from a scan of target potential. This is a straightforward approach and has been shown before[48], however it brings an additional challenge of using the ToF analyser for imaging: instead of acquiring images at a few selected V_T values for each metastable ion of interest, V_T scans over at least a 50 V window would be required for each ion and each pixel. This makes it difficult to image samples with specific V_T values and spatially resolve isomers in the way it was done with the 90-degree deflection unit and Orbitrap analyser.

The ability to access structure-sensitive information through ion transmission opens a new analytical dimension for SIMS. By coupling this capability with high spatial resolution imaging, OrbiSIMS provides a platform for studying isomeric complexity directly at surfaces and interfaces. This approach has potential for applications in glycomics and polysaccharide mapping, lipid and metabolite imaging, biomaterials and biointerfaces. More broadly, the results suggest that engineering ion transmission conditions, rather than only improving mass resolution or fragmentation methods, represents a powerful and underexplored strategy for extracting structural information in OrbiSIMS MSI.

Methods

OrbiSIMS silver measurements

An instrument built-in silver reference sample was used. Datasets were acquired using an OrbiSIMS instrument (Hybrid SIMS, IONTOF GmbH) in single beam depth profiling mode using a 30 keV Bi_3^+ ion beam from a liquid metal ion source with an average primary ion beam current of 2 nA in a cycle time of 200 μs. The beam was set to scan an area of 342 × 342 μm² of which positively charged secondary ions were collected from the central 300 × 300 μm² of the crater. 70 × 70 pixels were used per scan, which resulted in a single injection per scan. The analyser extraction voltage was set at 2500, 2000 and 500 V (data in main text corresponds to 2000 V). The Orbitrap mass analyser was operated with 512 ms injection time and 512 ms transient time for a mass resolving power of 240,000 at *m/z* 200. For scanning the V_T, the He collision cell pressure was kept at 0.12 mbar in high collisional cooling mode and the target potential was varied automatically during acquisition. Details of method are described elsewhere[32]. Silver clusters were used to calibrate the Orbitrap *m/z* scale in both positive and negative polarities.

ToF-SIMS silver measurements

An instrument built-in silver reference sample was used. Datasets were acquired using an OrbiSIMS instrument (Hybrid SIMS, IONTOF GmbH). The Bi_3^+ beam in long pulses was used to clean the sample. Acquisition used a 30 keV Bi_3^+ ion beam, pulse width 55 ns, target current 1.5 pA,

https://doi.org/10.1038/s41467-026-78604-8

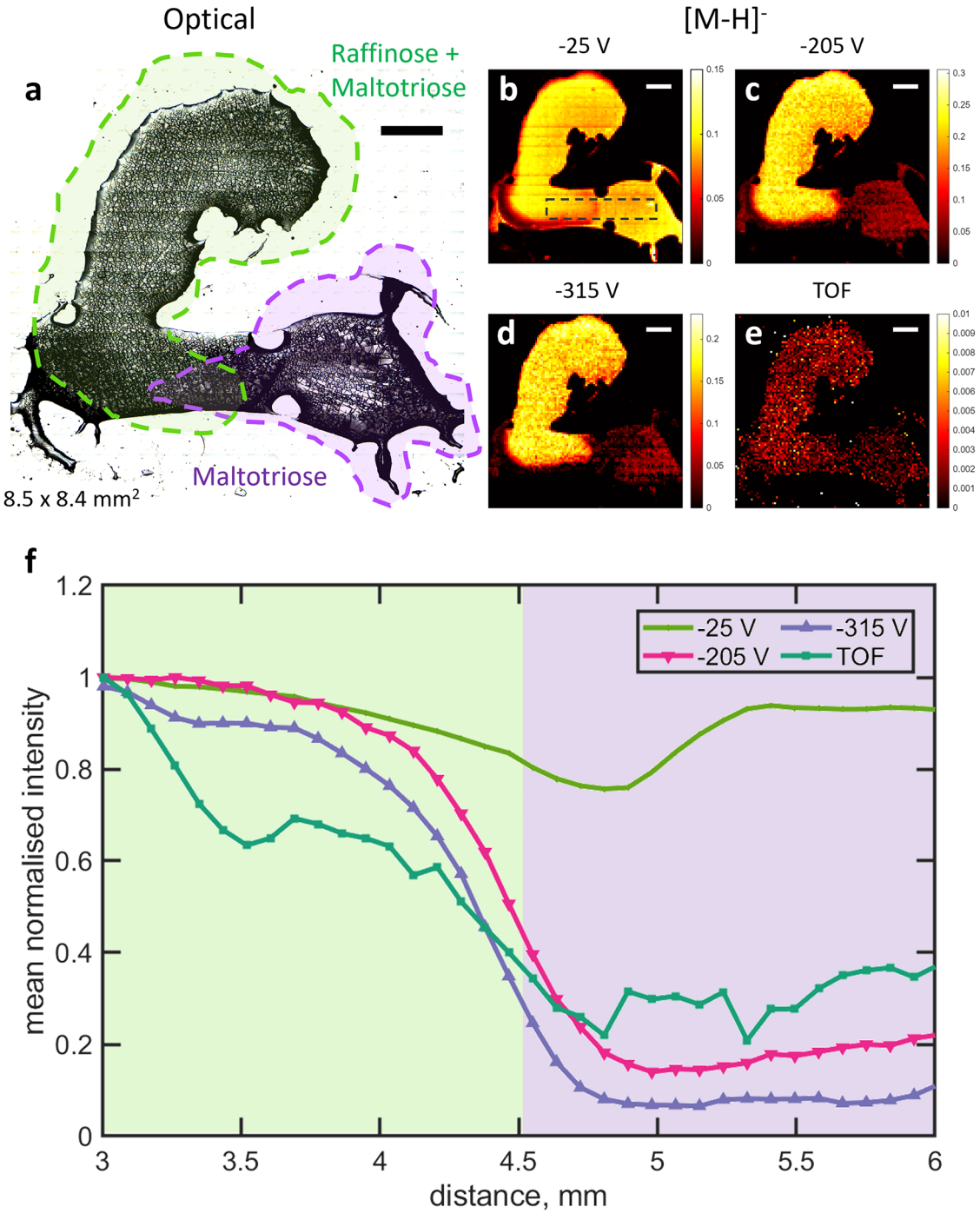


Fig. 4 | Spatially distinguishing structural isomeric trisaccharides. a optical image and indication of the raffinose + maltotriose (green) and maltotriose (purple) areas, **b**–**e** The intensity of the $[M\text{-}H]^-$ ion as V_T is changed Intensities are normalised using the total ion image. **e** The ToF-SIMS image, normalised against total ion count. **f** An area profile (represented by black dashed rectangle in (**b**)) comparing the spatial differences in intensity for the images in (**b**–**e**). The scale bars in (**a**–**e**) correspond to 1 mm. Source data are provided as a Source Data file.

cycle time of 150 μs for a mass range of 2133 u. Acquisition area 400 × 400 μm², 128 × 128 pixels, 1 shot per pixel per frame, 20 scans. The wide pulse width reduced the measurement time at the expense of mass resolution. Analyser extraction voltage −2 kV for positive ions. For the changing target potential, the reflectron potential was 20 V to optimise ion transmission and mass resolution. Each voltage was allowed to settle for at least 3 s before the acquisition started. Each results file was individually calibrated. The peak list was the same for all measurements and covered the width each set of isotopologues for a given $[Ag_n]^+$ cluster.

Ion optics simulation framework

The ion optics model was made using SIMION. The model contains a biased sample holder, an extraction cone, one set of einzel lenses for focusing of secondary ions and a hemispherical analyser (SI switch) to deflect the secondary ions by 90 degrees into the transfer system to the Orbitrap (Fig. 1a). With this set up it is possible to simulate V_T scans for secondary ions of arbitrary kinetic energy of formation, angular distribution and mass spectrum. We have also incorporated a user program to simulate decays and, by comparing against experimental data, the simulation framework may help to determine where the

decays may occur within the system. To benchmark simulations against experiments, we simulated a V_T scan of $[Ag_{13}]^+$ ions that can decay to $[Ag_{12}]^+$ and subsequently to $[Ag_{11}]^+$ (Fig. 1e). For this simulation, dissociation only occurs between the exit of the einzel lens the entrance to the 90 degrees deflection unit, which is a field-free region and thus satisfies the hypothesis of Eq. (1). The extraction potential was set at −2000 V and the deflection unit potential difference was set at 720 V. The initial spatial and kinetic energy distributions of the $[Ag_{13}]^+$ ions and probabilities of decay were set arbitrarily. More details are in Supplementary Note 3.

Trisaccharides samples preparation for OrbiSIMS

For the first sample set, substrate Si wafers (SiO_2/Si) were prepared by sonication in IPA (isopropyl alcohol) followed by a wipe cleaning using lint free paper (Kimtech). The final step of the cleaning was performed using a UV ozone cleaner (T10X10/OES/E from UVOCS INC). Analytical standards of raffinose, maltotriose and melezitose (Sigma Aldrich/Merck product IDs 95068, 07304 and 851493). Each powder was dissolved in DI water (10 mM) and spin-coated using a programmable spin coater (Laurel technologies corporation model WS-400/500B lite series). Spin-coating parameters for the trisaccharide solution was set at 1500 RPM for a duration of 3 min onto UV-ozone cleaned silicon wafer substrates using 100 μL of the solution. For mixtures, 1:1 and 1:2 raffinose:maltotriose in solution, the same deposition method was applied.

A second sample set was prepared using raffinose and maltotriose at approximately 0.16 M concentration, drop coated onto a cleaned silicon substrate. (IPA sonification, DI water sonification and IPA again followed by ozone cleaning as above.) One set of measurement was taken on separated drops of raffinose and maltotriose, on the same silicon substrate, over a rectangular area of 0.4 × 4.0 mm. Another measurement set was a maltotriose drop drawn down in a streak along the silicon substrate and allowed to dry. The raffinose drop was then added and using the tip of the pipette the raffinose was drawn down to join the previously dropped and dried maltotriose (Fig. 4a).

OrbiSIMS trisaccharides measurements

Datasets were acquired using an OrbiSIMS instrument (Hybrid SIMS, IONTOF GmbH). Depth profiles were obtained in a single beam mode using a 20 keV Ar_{2800}^+ ion beam from a gas cluster ion source. The secondary ions extraction voltage was set at 2 keV. The average primary ion beam current was 24 pA in a cycle time of 200 μs (trisaccharides). For each initial spectra measurements, the beam was set to scan areas of 543 × 543 μm² of which negatively charged secondary ions were collected from the central 500 × 500 μm² of the crater. For each scan, 70 × 70 pixels were used, which resulted in a single injection per scan. Analysis of secondary ions using the Orbitrap mass analyser with 512 ms injection time, 512 ms transient time for a mass resolving power of 240,000 at *m/z* 200 and an *m/z* range between 100 and 1500. For V_T scans, the He collision cell pressure was kept at 0.04 mbar in low collisional cooling mode and the target potential was varied automatically during acquisition. For p_{He} scans, V_T was fixed and the collision cell pressure was varied continuously. Details of the method are described elsewhere[32]. For the imaging experiments, a 20 keV Ar_{3000}^+ with a spot size of approximately 5 μm was used. The beam current was set at 26 pA with a duty cycle of 31.2% of a cycle time of 100 μs. Each image was acquired over areas of 400 × 400 μm² with pixel sizes of 4 μm. For large area Orbitrap images, the area imaged was 8.5 × 8.4 mm² with a patch size of 400 × 400 μm². The pixels per patch varied from 20 × 20 to 10 × 10. A 20 keV Ar_{3500}^+ primary ion beam with a spot size of approximately 5 μm was used. The Orbitrap analyser settings changed to an injection time of 50 ms and a mass resolution of 30,000 at *m/z* 200 and an *m/z* range between 100 and 1000. The reduction in mass resolution and pixel density allowed an imaging time of approximately 30 min per large scale image. Argon gas flooding and the flood gun were used to minimise charge build-up and the He collision cell pressure was kept at 0.04 mbar in low collisional cooling mode.

The ToF images used a 30 keV Bi_3^+ primary beam, with a pixel density of 100 pixels per mm. The image area was identical to the previous large-scale Orbitrap image area.

IMS sample preparation

Each trisaccharide powder sample was dissolved in CH_3CN:H_2O 9:1 (v/v) containing 0.1% v/v ammonia to 0.1 μmol/mL.

IMS experiment

Each sample solution was directly infused into Synapt G2-Si HDMS instrument with Travelling Wave Ion Mobility Spectrometry (TWIMS) function (Waters, UK) through a chip-based nano-electrospray source (TriVersa NanoMate, Advion, US). The cone voltage and source temperature were set to 80 V and 100 °C, respectively. The nitrogen drift gas flow was set at 90 mL/min for all TWIMS experiments. The traveling wave speed was set to 900 m/s and the wave height set at 40 V. Mass spectra and ion mobility spectra were processed using MassLynx V4.1 (Waters, UK).

Data analysis: V_T spectra and p_{He} scans

OrbiSIMS data was exported from SurfaceLab 7.3 (IONTOF GmbH) as scan-resolved intensities for a series of mass spectra peaks. For each scan, a parameter (target potential (V_T) or helium pressure (p_{He})) was associated with it. Datasets were then converted into parameter vs. intensity using MATLAB R2023a. **Peak fitting of** Fig. 3g: fitting was done in specific windows of V_T values. The general model used considered three Gaussian peaks (B_{1-3}, zm_{1-3}, s_{1-3}), an exponential decay background (b_0, b_1) and an offset (b_2):

$$f(x) = B_1 \cdot e^{-((x-zm_1)/s_1)2} + B_2 \cdot e^{-((x-zm_2)/s_2)2} + B_3 \cdot e^{-((x-zm_3)/s_3)2} + b_0 \cdot e^{b_1 x} + b_2$$

Initial conditions were set based on the signal of the pure samples of raffinose (B1 and B2 amplitudes) and maltotriose (B3 amplitude). Fitting was done using MATLAB's "fit" function using a robust nonlinear least squares algorithm. The V_T spectra for *m/z* 179.0562 $[C_6H_{11}O_6]^-$ was chosen as it presented distinct features for both sugars within the V_T fitting window from −285 to −405 V.

OrbiSIMS imaging

For each ion image, data was exported from SurfaceLab as ASCII files containing intensity information for each pixel. Intensity maps were then generated using MATLAB R2023a.

Data availability

All OrbiSIMS data reported in this manuscript have been deposited as. imzML and. ibd files and IMS data reported in this manuscript have been deposited as an xlsx file to figshare (https://doi.org/10.6084/m9.figshare.28892756). Source data are provided with this paper.

Code availability

imzML files can be processed in MATLAB using the imzML parser of SpectralAnalysis (https://github.com/AlanRace/SpectralAnalysis). This manuscript did not require the development of code that is central to the main work described.

References

1. Isomerism in organic compounds and drug molecules: chemistry and significance in biology. In *Basic Chemistry for Life Science Students and Professionals* 149–194 https://doi.org/10.1039/9781839168086-00149 (The Royal Society of Chemistry, 2023).
2. Chatgilialoglu, C., Ferreri, C., Melchiorre, M., Sansone, A. & Torreggiani, A. Lipid geometrical isomerism: from chemistry to biology and diagnostics. *Chem. Rev.* **114**, 255–284 (2014).

3. Hamilton, B. S. et al. A library of chemically defined human N-glycans synthesized from microbial oligosaccharide precursors. *Sci. Rep.* **7**, 15907 (2017).
4. Varki, A. et al. *Essentials of Glycobiology [Internet]* 3rd ed. Cold Spring Harbor (NY): Cold Spring Harbor Laboratory Press; 2015–2017 (2022).
5. Lockyer, N. P. et al. Secondary ion mass spectrometry. *Nat. Rev. Methods Prim.* **4**, 32 (2024).
6. Fletcher, J. S. et al. A new dynamic in mass spectral imaging of single biological cells. *Anal. Chem.* **80**, 9058–9064 (2008).
7. Fisher, G. L., Hammond, J. S., Larson, P. E., Bryan, S. R. & Heeren, R. M. A. Parallel imaging MS/MS TOF-SIMS instrument. *J. Vac. Sci. Technol. B, Nanotechnol. Microelectron. Mater. Process. Meas. Phenom.* **34**, 03H126 (2016).
8. Newell, C. L., Vorng, J. L., MacRae, J. I., Gilmore, I. S. & Gould, A. P. Cryogenic OrbiSIMS localizes semi-volatile molecules in biological tissues. *Angew. Chemie - Int. Ed.* **59**, 18194–18200 (2020).
9. Zhang, J. et al. Cryo-OrbiSIMS for 3D molecular imaging of a bacterial biofilm in its native state. *Anal. Chem.* **92**, 9008–9015 (2020).
10. Ward, S. et al. Integrating cryo-OrbiSIMS with computational modelling and metadynamics simulations enhances RNA structure prediction at atomic resolution. *Nat. Commun.* **15**, 4367 (2024).
11. Passarelli, M. K. et al. The 3D OrbiSIMS—label-free metabolic imaging with subcellular lateral resolution and high mass-resolving power. *Nat. Methods* **14**, 1175–1183 https://doi.org/10.1038/nmeth.4504 (2017).
12. Kotowska, A. M. et al. Protein identification by 3D OrbiSIMS to facilitate in situ imaging and depth profiling. *Nat. Commun.* **11**, 5832 (2020).
13. Kotowska, A. M. Enabling in situ protein analysis for pharmaceutical applications using 3D OrbiSIMS University of Nottingham (United Kingdom), 2021 (2021).
14. Kotowska, A. M. et al. Surface lipids in nematodes are influenced by development and species-specific adaptations. *J. Am. Chem. Soc.* **147**, 6439–6449 (2025).
15. Kotowska, A. et al. Molecular orientation and stratification revealed in RNA-lipid nanoparticles using cryogenic orbitrap secondary ion mass spectrometry (Cryo-OrbiSIMS). https://doi.org/10.26434/chemrxiv-2025-zxkf1 (2025).
16. He, W. et al. Untargeted metabolomic characterization of glioblastoma intra- tumor heterogeneity using OrbiSIMS. *Anal. Chem.* **95**, 5994–6001 https://doi.org/10.1021/acs.analchem.2c05807 (2023).
17. Suvannapruk, W. et al. Single-cell metabolic profiling of macrophages using 3D OrbiSIMS: correlations with phenotype. *Anal. Chem.* **94**, 9389–9398 https://doi.org/10.1021/acs.analchem.2c01375 (2022).
18. Zani, F. et al. The dietary sweetener sucralose is a negative modulator of T cell-mediated responses. *Nature* **615**, 705–711 (2023).
19. Franchet, A. et al. An intercellular metabolic relay for brain sparing in Drosophila https://doi.org/10.1101/2025.04.02.645514 (2025).
20. Ruotolo, B. T. et al. Ion mobility–mass spectrometry reveals long-lived, unfolded intermediates in the dissociation of protein complexes. *Angew. Chemie Int. Ed.* **46**, 8001–8004 (2007).
21. Hall, Z., Politis, A., Bush, M. F., Smith, L. J. & Robinson, C. V. Charge-state dependent compaction and dissociation of protein complexes: insights from ion mobility and molecular dynamics. *J. Am. Chem. Soc.* **134**, 3429–3438 (2012).
22. Konermann, L., Rodriguez, A. D. & Liu, J. On the formation of highly charged gaseous ions from unfolded proteins by electrospray ionization. *Anal. Chem.* **84**, 6798–6804 (2012).
23. Dobo, A. & Kaltashov, I. A. Detection of multiple protein conformational ensembles in solution via deconvolution of charge-state distributions in ESI MS. *Anal. Chem.* **73**, 4763–4773 (2001).
24. Holčapek, M., Jirásko, R. & Lísa, M. Recent developments in liquid chromatography–mass spectrometry and related techniques. *J. Chromatogr. A* **1259**, 3–15 (2012).
25. Böcker, S. Searching molecular structure databases using tandem MS data: are we there yet? *Curr. Opin. Chem. Biol.* **36**, 1–6 (2017).
26. Hernandez, P., Müller, M. & Appel, R. D. Automated protein identification by tandem mass spectrometry: Issues and strategies. *Mass Spectrom. Rev.* **25**, 235–254 (2006).
27. Johnson, A. R. & Carlson, E. E. Collision-induced dissociation mass spectrometry: a powerful tool for natural product structure elucidation. *Anal. Chem.* **87**, 10668–10678 (2015).
28. Snyder, D. T., Harvey, S. R. & Wysocki, V. H. Surface-induced dissociation mass spectrometry as a structural biology tool. *Chem. Rev.* **122**, 7442–7487 (2022).
29. Narang, D., Lento, C. & J. Wilson, D. HDX-MS: an analytical tool to capture protein motion in action. *Biomedicines* **8**, 224 (2020).
30. Gabelica, V. & Marklund, E. Fundamentals of ion mobility spectrometry. *Curr. Opin. Chem. Biol.* **42**, 51–59 (2018).
31. Van Nuffel, S. & Brunelle, A. TOF-SIMS Imaging of Biological Tissue Sections and Structural Determination Using Tandem MS. In *Mass Spectrometry Imaging of Small Molecules*. (eds Lee,Y. J.) Methods in Molecular Biology, vol 2437. https://doi.org/10.1007/978-1-0716-2030-4_5 (Humana, New York, NY. 2022).
32. Matjacic, L. et al. OrbiSIMS metrology part I: optimisation of the target potential and collision cell pressure. *Surf. Interface Anal.* **54**, 331–340 https://doi.org/10.1002/sia.7058 (2022).
33. Delcorte, A. & Bertrand, P. Metastable decay of molecular fragment ions sputtered from hydrocarbon polymers under keV ion bombardment. *Int. J. Mass Spectrom.* **184**, 217–231 (1999).
34. Shard, A. A. G. & Gilmore, I. S. Analysis of metastable ions in the ToF-SIMS spectra of polymers. *Int. J. Mass Spectrom.* **269**, 85–94 (2008).
35. Forst, W. & Tardy, D. C. Theory of unimolecular reactions. *Phys. Today* **27**, 57–58 (1974).
36. Schueler, B. et al. Unimolecular decay measurements of secondary ions from organic molecules by time-of-flight mass spectrometry. *Int. J. Mass Spectrom. Ion Process.* **92**, 185–194 (1989).
37. Zubarev, R. A., Abeywarna, U., Håkansson, P., Demirev, P. & Sundqvist, B. U. R. Kinetic energies of secondary ions in MeV and keV particle-induced desorption. *Rapid Commun. Mass Spectrom.* **10**, 1966–1974 (1996).
38. Delcorte, A. et al. Desorption/ionization of molecular nanoclusters: SIMS versus MALDI. *Appl. Surf. Sci.* **231-232**, 131–135 (2004).
39. Shard, A. G. & Gilmore, I. S. Analysis of metastable ions in the ToF-SIMS spectra of polymers. *Int. J. Mass Spectrom.* **269**, 85–94 (2008).
40. Alamanova, D., Grigoryan, V. G. & Springborg, M. Theoretical study of the structure and energetics of silver clusters. *J. Phys. Chem. C* **111**, 12577–12587 (2007).
41. Lee, J., Chai, M. & Bleiholder, C. Differentiation of isomeric, non-separable carbohydrates using tandem-trapped ion mobility spectrometry–mass spectrometry. *Anal. Chem.* https://doi.org/10.1021/acs.analchem.2c02844 (2022).
42. Varki, A. et al. Symbol nomenclature for graphical representations of glycans. *Glycobiology* **25**, 1323–1324 (2015).
43. Neelamegham, S. et al. Updates to the symbol nomenclature for glycans guidelines. *Glycobiology* **29**, 620–624 (2019).
44. Reinhold, V. N. & Carr, S. A. New mass spectral approaches to complex carbohydrate structure. *Mass Spectrom. Rev.* **2**, 153–221 (1983).
45. Milne, L. K. et al. Validation of the use of ToF-SIMS for analysis of glycosaminoglycans. *Carbohydr. Polym.* **371**, 124415 (2026).

46. Shard, A. G., Spencer, S. J., Smith, S. A., Havelund, R. & Gilmore, I. S. The matrix effect in organic secondary ion mass spectrometry. *Int. J. Mass Spectrom.* **377**, 599–609 (2015).
47. Mizomichi, K., Yamagishi, T., Kawashima, T., Dürr, M. & Aoyagi, S. Investigating matrix effects of different combinations of lipids and peptides on TOF-SIMS data. *Biointerphases* **15**, 021008 (2020).
48. Delcorte, A. & Poleunis, C. Mechanistic Insight into gas cluster-induced sputtering of kilodalton molecules using kinetic energy distribution measurements **123**, 19704–19714 https://doi.org/10.1021/acs.jpcc.9b05363 (2019).
49. Wysocki, V. H., Jones, J. L. & Ding, J. M. Polyatomic ion/surface collisions at self-assembled monolayers films. *J. Am. Chem. Soc.* **113**, 8969–8970 (1991).
50. Campbell, D. I., Ferreira, C. R., Eberlin, L. S. & Cooks, R. G. Improved spatial resolution in the imaging of biological tissue using desorption electrospray ionization. *Anal. Bioanal. Chem.* **404**, 389–398 (2012).
51. Yin, R., Burnum-Johnson, K. E., Sun, X., Dey, S. K. & Laskin, J. High spatial resolution imaging of biological tissues using nanospray desorption electrospray ionization mass spectrometry. *Nat. Protoc.* **14**, 3445–3470 (2019).
52. Niehaus, M., Soltwisch, J., Belov, M. E. & Dreisewerd, K. Transmission-mode MALDI-2 mass spectrometry imaging of cells and tissues at subcellular resolution. *Nat. Methods* **16**, 925–931 (2019).
53. Hale, O. J. & Cooper, H. J. In situ mass spectrometry analysis of intact proteins and protein complexes from biological substrates. *Biochem. Soc. Trans.* **48**, 317–326 (2020).
54. Qiu, Q. et al. Distribution analysis of salvianolic acids in myocardial ischemic pig tissues by automated liquid extraction surface analysis coupled with tandem mass spectrometry. *Evid. Based Complement. Altern. Med.* **2020**, 8476794 (2020).
55. McGee, J. P. et al. Automated imaging and identification of proteoforms directly from ovarian cancer tissue. *Nat. Commun.* **14**, 6478 (2023).
56. Bruinen, A. L., Fisher, G. L. & Heeren, R. M. A. ToF-SIMS Parallel Imaging MS/MS of Lipid Species in Thin Tissue Sections. In *Imaging Mass Spectrometry. Methods in Molecular Biology*, (eds Cole, L.) vol 1618. https://doi.org/10.1007/978-1-4939-7051-3_14 (Humana Press, New York, NY. 2017).
57. Trindade, G. F. et al. High-performance analysers in SIMS. In *Secondary Ion Mass Spectrometry* 133–158 https://doi.org/10.1039/9781837674763-00133 (Royal Society of Chemistry, 2025).

Acknowledgements

The authors would like to thank Dr Alexander Shard and Dr Lily Ellis-Gibbings from the UK National Physical Laboratory (NPL) for respectively insightful discussion about ion dissociation and conducting an internal technical review. Microsoft Copilot was used to review and/or refine parts of the text.

Author contributions

All authors contributed to the manuscript and approved the final manuscript. The concept was devised by G.F.T., A.P. and I.S.G. G.F.T., M.M., A.E. and R.P. acquired OrbiSIMS and ToF-SIMS experimental data with advice from G.F.T., A.P., I.S.G., C.L.N. and J.F.W. R.P. and G.F.T. developed the ion optics simulation framework. G.F.T., M.M., A.E., A.P. and I.S.G. processed and interpreted OrbiSIMS and ToF-SIMS data. CLN conducted a literature review of MS methods for structural analysis. BY proposed the trisaccharide isomer samples, acquired and interpreted IMS data. J.L.V., M.M. and G.F.T. prepared spin-coated samples. M.M. prepared drop coated samples with guidance from A.E. and C.L.N. G.F.T. oversaw the study.

Funding

M.M., R.P., B.Y., A.E., J.L.V., I.S.G. and G.F.T. disclose support for by the UK National Measurement System (NMS). N.P.L. is operated by NPL Management Ltd, a wholly-owned company of the UK Government. M.M. and J.F.W. disclose support by UK Research and Innovation (UKRI) by way of an Engineering and Physical Sciences Research Council (EPSRC) Industrial CASE Award with NPL. C.L.N., A.E., I.S.G. and G.F.T. disclose support by a Wellcome Trust Technology Development Grant (grant number 104566). This work was supported by funding from the Francis Crick Institute, which receives its core funding from Cancer Research UK (CC2101), the UK Medical Research Council (CC2101) and the Wellcome Trust (CC2101). A.P. declares no relevant funding.

Competing interests

The authors declare the following competing financial interest: A.P. is an employee of IONTOF GmbH, the manufacturer of the OrbiSIMS instrument used in this research. The remaining authors declare no competing interests.

Additional information

Supplementary information The online version contains supplementary material available at https://doi.org/10.1038/s41467-026-78604-8.

Correspondence and requests for materials should be addressed to Ian S. Gilmore or Gustavo F. Trindade.

Peer review information *Nature Communications* thanks Sebastiaan van Nuffel, Frank Sobott, and the other, anonymous, reviewer(s) for their contribution to the peer review of this work. A peer review file is available.

Reprints and permissions information is available at http://www.nature.com/reprints

Publisher's note Springer Nature remains neutral with regard to jurisdictional claims in published maps and institutional affiliations.

Open Access This article is licensed under a Creative Commons Attribution 4.0 International License, which permits use, sharing, adaptation, distribution and reproduction in any medium or format, as long as you give appropriate credit to the original author(s) and the source, provide a link to the Creative Commons licence, and indicate if changes were made. The images or other third party material in this article are included in the article's Creative Commons licence, unless indicated otherwise in a credit line to the material. If material is not included in the article's Creative Commons licence and your intended use is not permitted by statutory regulation or exceeds the permitted use, you will need to obtain permission directly from the copyright holder. To view a copy of this licence, visit http://creativecommons.org/licenses/by/4.0/.

© The Author(s) 2026